J Opt (December 2023) 52(4):1621–1627
https://doi.org/10.1007/s12596-022-00930-z

RESEARCH ARTICLE

Structural, Morphological, Photoluminescence, and sensitivity of Au:TiO_2 nanoparticles via laser ablation on porous silicon

Eman M. Sulaiman[1] · **Uday M. Nayef**[1] · **Falah A. H. Mutlak**[2]

Received: 1 May 2022 / Accepted: 9 July 2022 / Published online: 29 July 2022

Abstract In this study, a novel, simple method has been used for fabricated of Au:TiO_2 nanoparticles. The manufacture consisted of two steps: first, ablating a gold (Au) target immersed in CTAB solution to produce colloidal Au NPs and then inserting a titanium (Ti) target in the solution to prepare Au:TiO_2 NPs via laser ablation in liquid (LAL) at various laser energies. Then, it was placed on porous-Si (PS). PS is made by etching n-type crystalline c-Si wafers by photo-electrochemical etching (PECE). The XRD, TEM, AFM, PL analyses were employed to characterize the samples. Lastly, the impact of varying operation temperature of hydrogen sulfide (H_2S) and nitrogen dioxide (NO_2) gas sensors fabricated from prepared specimens on the sensors sensitivity, response time, and time to recover was explored. We found the greatest sensitivity of Au:TiO_2 NPs/PS when ablated at 1000 mJ. The synthesized Au/TiO_2 NPs thin films show high sensitivity 94.12% and 42.69% with fast response and recovery of H_2S and NO_2 gas at for low concentration 12.6 and 64.5 ppm, respectively.

Keywords Au:TiO_2 nanoparticles · Porous silicon · Laser ablation · Gas sensor

Introduction

Nano-materials are used to manufacture devices such as gas sensors, photo-detector, and solar cell, due to the quantum confinement effect, low cost, easy fabrication, large active area, and charge transport [1–4].

Gas sensor is an instrument that detects the presence of various gases in an area, particularly those that are potentially dangerous to humans and animals. In recent years, the development of gas sensor technologies for monitoring environmental contamination has gotten a lot of attention [5].

The characteristics of the sensing materials used are well recognized to influence chemical gas sensor performance parameters such as selectivity, temporal response, sensitivity, stability, durability, and repeatability [6]. The specific surface of sensing materials has a significant impact on chemical gas sensor sensitivity. The sensor sensitivity increases as the specific surface of the detecting material increases [7–9]. Semiconductor and metallic nanoparticles gas sensors continue to play an important part in their applications [10]. Because of their low cost, distinctive structure, ease of production, and outstanding physicochemical characteristics, transition metal oxide semiconductor substances like TiO_2, ZnO, and CuO are a potential class of sensors [11–14].

TiO_2 is an n-type semi-material with a high resistance and a band gap of roughly 3.2 eV. It has gained a lot of attention for its use in gas sensors, photo-catalysis, and solar cells [10, 15]. This semiconductor of n-type has been investigated to employ in the sensing of H_2S; it is produced in significant amount from both human and natural processes, particularly in crude oil refineries with the extraction of acid natural gas [17–19].

Inhaling H_2S has been demonstrated to have significant health consequences on the respiratory system; also, H_2S poisons the human body and can cause death at concentrations greater than 250 ppm [20, 21].

Other desirable characteristics of TiO_2 include its strong photocatalytic activity, superior chemical and physical

✉ Uday M. Nayef
unayef@yahoo.com

[1] Department of Applied Science, University of Technology, Baghdad, Iraq

[2] College of Science, Department of Physics, University of Baghdad, Baghdad, Iraq

stability, ease of oxygen adsorption on its surface, ease of preparation, and low cost. Because of its excellent application stability, TiO_2 offers a lot of potential for NO_2 gas sensing [22].

NO_2 is a harmful air pollutant for plants and the respiratory systems of humans and animals. Furthermore, NO_2 emissions have resulted in major environmental issues such as acid rain and photochemical smog [23, 24]. The development of inexpensive, small, sensitive, and reliable gas sensors to monitor and manage NO_2 gas concentrations from automobiles and industrial processes is critical to preserve human life [25, 26].

Laser ablation of large materials in a liquid medium is a common, simple, and cost-effective method for formation nanoparticles [27, 28]. Throughout the laser ablation in solution approach, a high-power laser pulse was focused on the face of a bulk object submerged in a solution. Ionization, atomization, and decomposition of the target are all caused by irradiation [27, 29].

In this study, Au:TiO_2 NPs can be combined using laser ablation in a liquid medium, after that deposited on porous-Si, employed for gas sensor applications.

Experimental details

The Au:TiO_2 NPs were made using the laser ablation process: firstly we put the plate of gold in the bottom of a glass container which filled by 3 mL of CTAB solution. Ablation of plate was carried out by a single 100 pulse at 1064 nm wave length with laser energy 600, 800 and 1000 mJ. Following the ablation technique for validating Au NPs generation, a Ti target was placed in a glass vial containing an Au NPs solution and ablated by the same condition of preparation Au NPs, after that the Au:TiO_2 NPs colloids solution was obtained.

Secondly, we formed PS by using the PECE method [30] from n-type silicon wafer with resistivity of 1.5–4 Ω.cm. PEACE has been obtained via etching a silicon plate in 16 percent HF (hydrofluoric acid) as the electrolyte for 15 min at a current density of 12 mA/cm^2 and illuminating with a halogen beam. In the last step, Au:TiO_2 suspension dropped on this PS.

Results and discussion

The phases and grain size are determined via XRD analysis. XRD pattern for the examined Au:TiO_2 specimen, which was generated via PLAL in CTAB solution at 800 mJ laser energy and then deposited on porous-Si substrate, is illustrated in Fig. 1. The XRD structure of the sample shows a strong peak of x-ray diffracted from the Si substrate at $2\theta = 69$◦. The XRD peaks for Au:TiO_2 NPs can be identified to (fcc) Au (JCPDS card No. 002–1095) and anatase TiO_2 (JCPDS card No. 21–1272).

The peaks were observed at $2\theta = 34.05°$, 44.4° correspond to the (110) and (200) planes of the cubic crystal of Au NPs, respectively. The TiO_2 NPs' XRD shows two distinct peaks at 37.28° and 62. 9°, which correspond to planes (004) and (204), respectively.

The structural characterization of the PS, Au:TiO_2 NPs/PS samples was analyzed using AFM as illustrated in Fig. 2. The surface of PS has a sponge-like structure with average diameter of 40.33 nm and average roughness of 24 nm as shown in Fig. 2A.

Figure 2B depicts Au:TiO_2 NPs completely filling or entirely covering PS pores. This is due to the surface PS layer's like-sponge morphology with a large surface region and

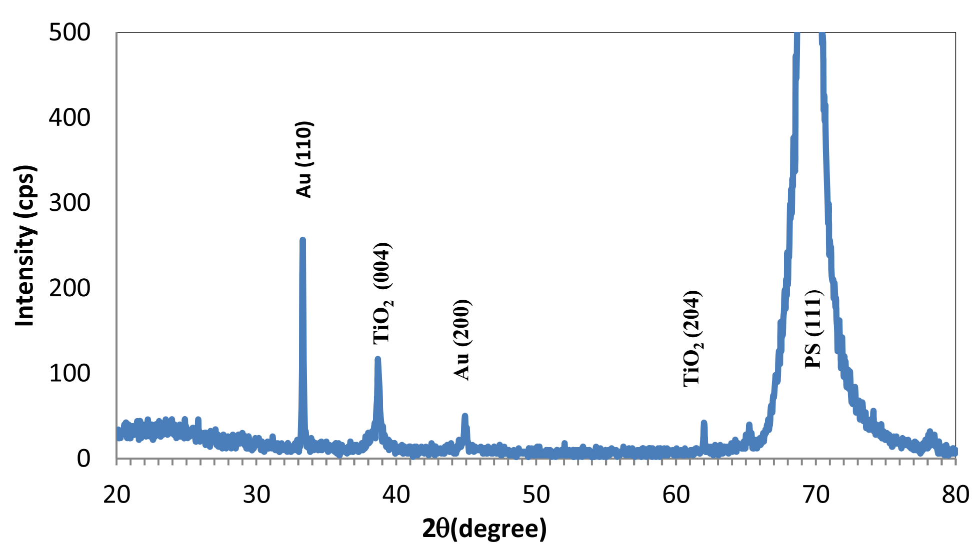

Fig. 1 XRD pattern of Au:TiO_2 NPs/PS laser ablated at 800 mJ on PS

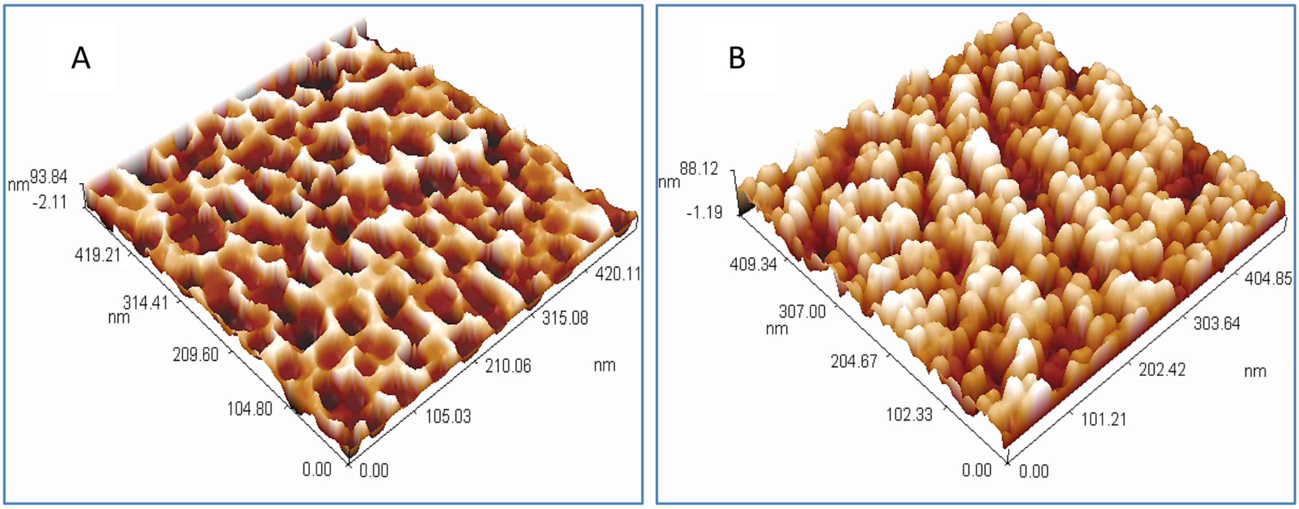

Fig. 2 3D AFM image for (**A**) PS, (**B**) Au:TiO_2 NPs/PS samples generated at 800 mJ/ 100 pulses deposited on PS

Table 1 The value of average rough nesses and diameter of PS and Au:TiO_2 NPs/PS samples

Samples	Average diameter (nm)	Average roughness(nm)
PS	40.33	24
Au:TiO_2 NPs/PS	30.44	17.7

a pores, which makes PS an adhesive substrate for allowing Au:TiO_2 NPs to enter its pores. As a result, the Au:TiO_2 NPs behaved like a transparent capping, which also given good coverage of a PS substrate, potentially improving the PS substrate's structural strength. The average roughness and diameter for Au:TiO_2 NPs/PS particles are shown in Table 1.

Figure 3 shows TEM images of Au:TiO_2NPs. Laser ablation with a laser energy of 800 mJ/pulse was used to generate Au:TiO_2 NPs. Au:TiO_2NPs, which are virtually spherical shape, with different in size from 7 to 55 nm, as can be observed. The creation of the core shell structures is confirmed by complementary contrast in TEM images. The Au NPs were responsible for the black core, whereas the TiO_2 shell was responsible for the grey color.

Photoluminescence (PL) studies provide knowledge on distinct energy states available between valence band and conduction band responsible for irradiative recombination.

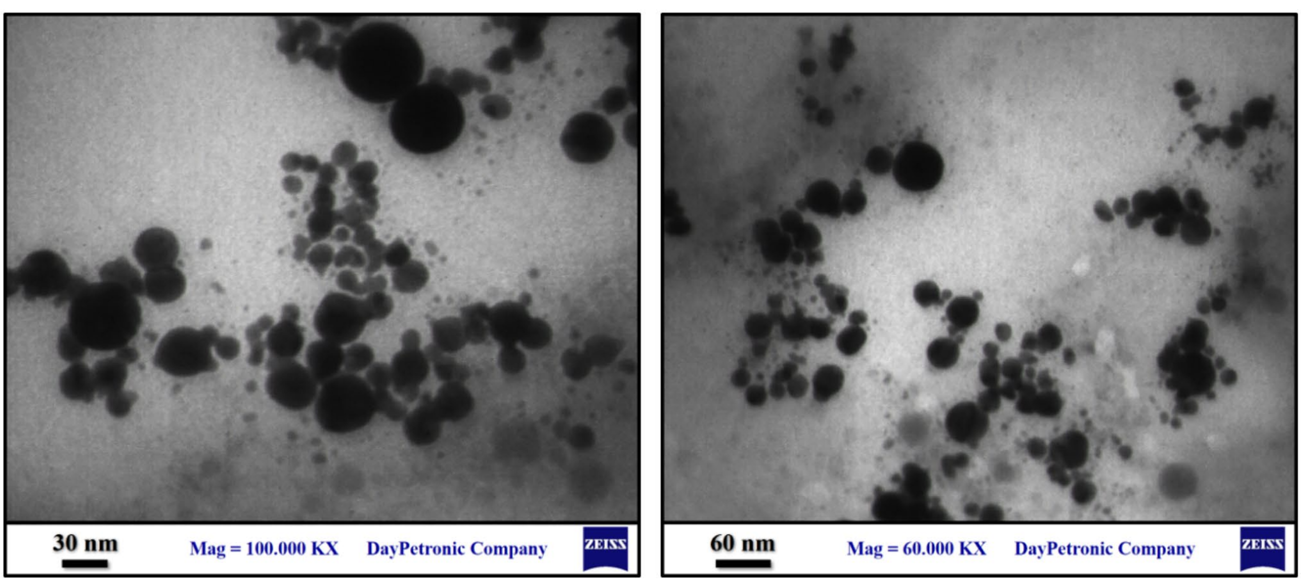

Fig. 3 TEM images of Au:TiO_2 NPs at different magnification images at (**a**) 30 nm and (**b**) 60 nm

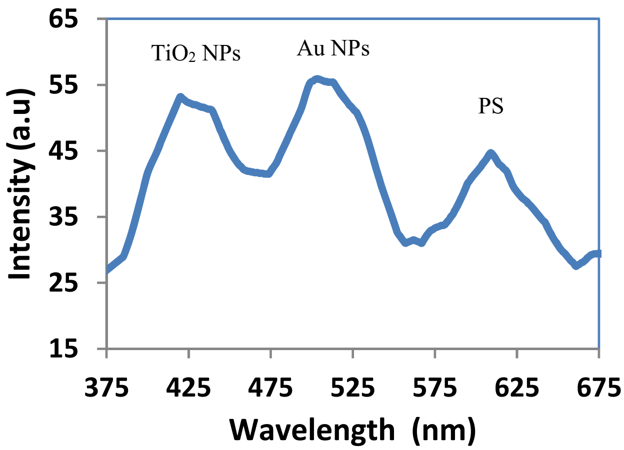

Fig. 4 Photoluminescence spectrum of (**A**) PS, **B** Au:TiO_2 NPs/PS

The PL spectra of Au:TiO_2 NPs prepared by laser ablation in ethanol solution deposited on PS substrate are shown in Fig. 4. The intensity of the photoluminescence spectra illumination of 602 nm is shown in Fig. 4, whereas the blue shift in a band gap depending on the Si wafer has been seen, because the last comes from quantum confinement effects (QCEs). The PL spectrum at room temperature for specimens Au:TiO_2 NPs/PS prepared PL bands at 350–550 nm on PS. The PL gave three peaks that were observed after the deposition of Au:TiO_2 NPs as compared to PS. Photoluminescence emission peaks at 417 nm (2.97 eV) which matched to the an anatase TiO_2 NPs at 497 nm corresponding to band edge of 2.5 eV for Au NPs PL spectral locations.

The quantum size effects from the Au:TiO_2 NPs are responsible for the significant blue-shift in the sharp peaks of plasmon absorption.

The sensor sensitivity is stated as ($S = (R_o - R_g) / R_g$), where R_g represents the sensor resistance when exposed to a test gas and R_o denotes the sensor resistance while exposed to air. Figure 5 displays the sensitivity of Au:TiO_2 NPs/PS thin prepared with the previously mentioned conditions by using the LAL technique for NO_2 and H_2S gases as a function of operating temperature. The figure illustrates

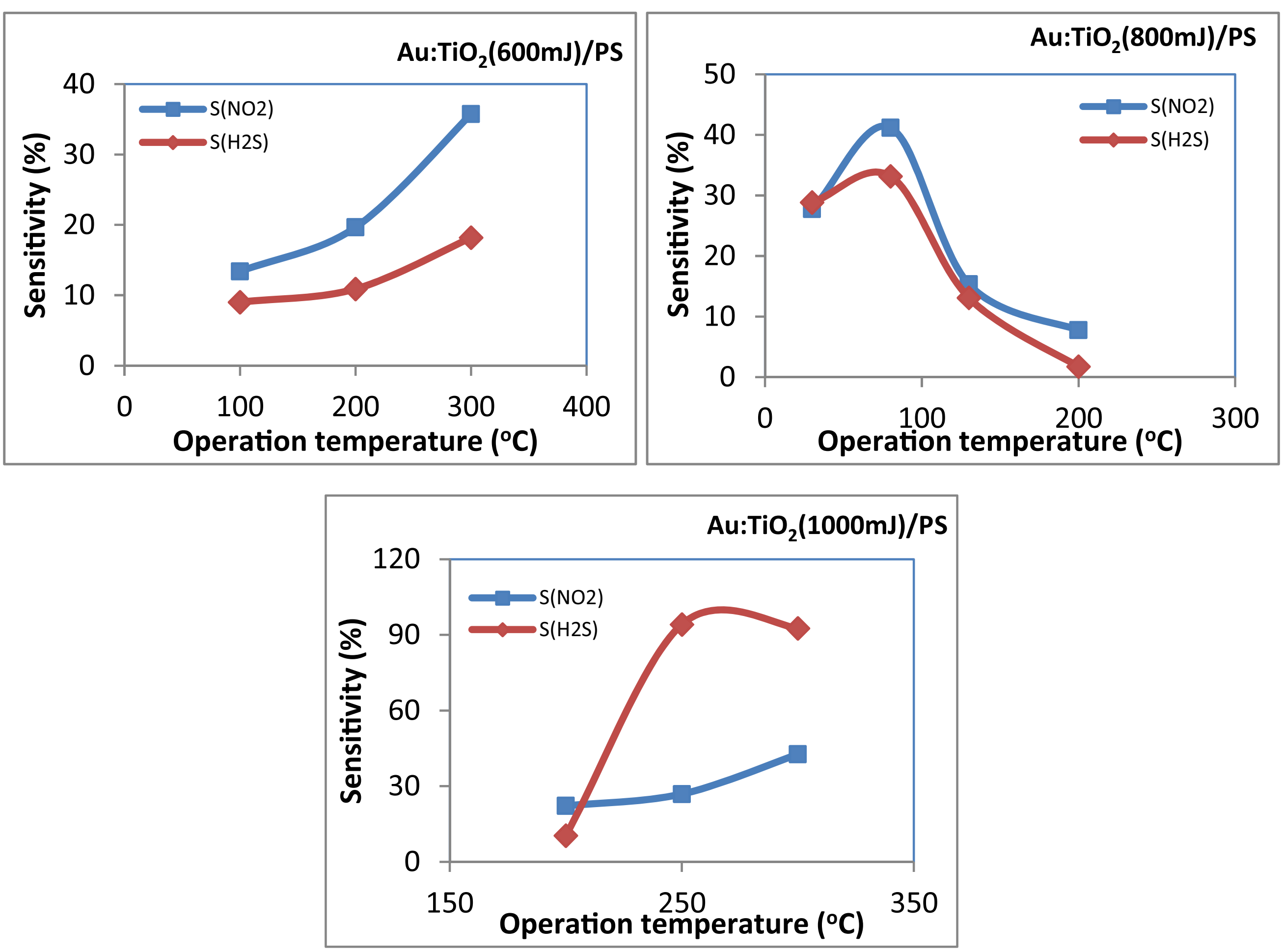

Fig. 5 Sensitivity as a function of the generated Au:TiO_2/PS gas sensor for H_2S and NO_2 gases at an operating temperature

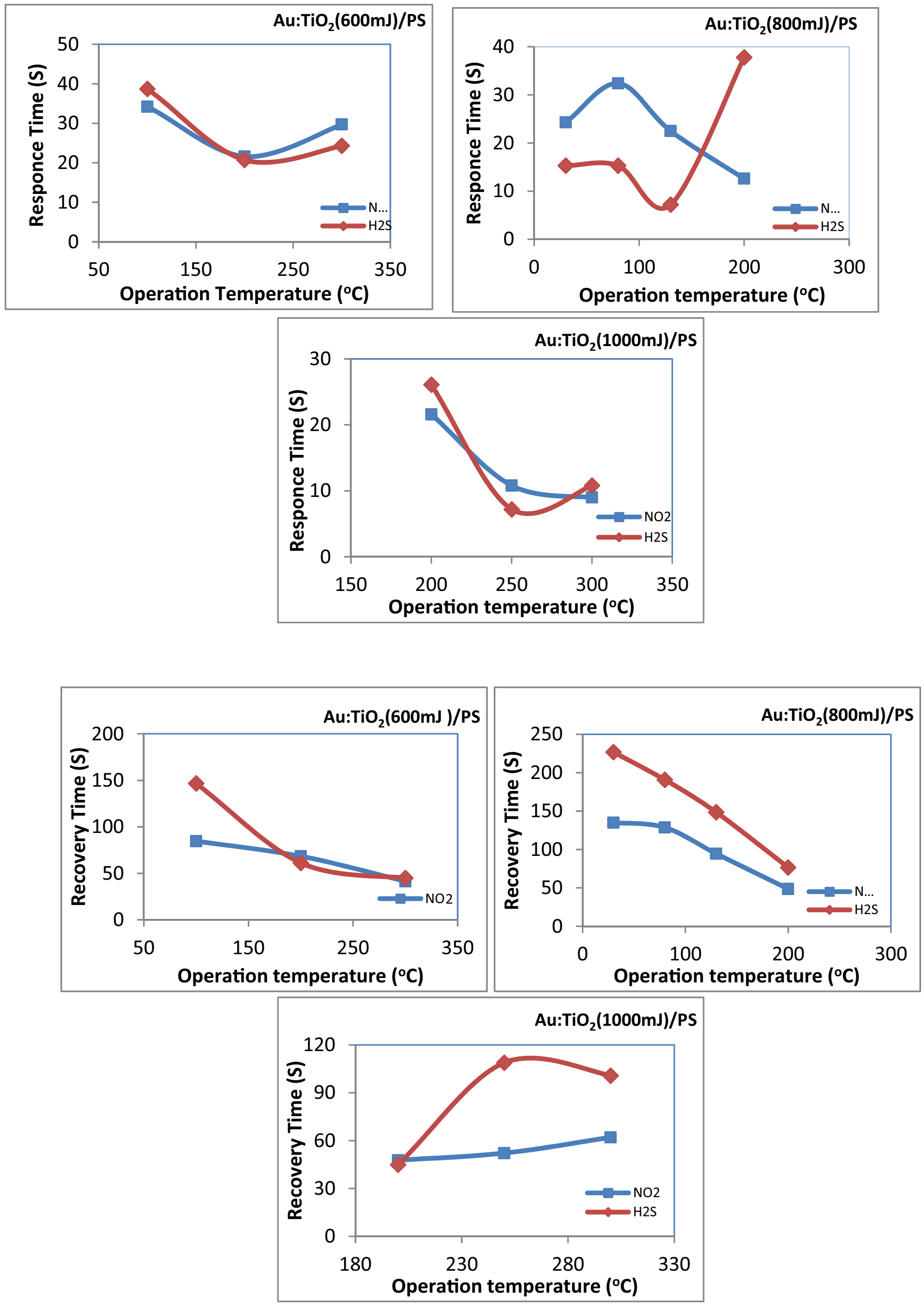

Fig. 6 Response and recovery period of Au:TiO_2 NPs/PS specimen formed with various energy lasers of 600, 800 and 1000 mJ.

that as the working temperature increases in the scope 30 – 300 °C, the sensitivity of H_2S and NO_2 gases increases. The Au:TiO_2/PS thin film at 1000 mJ have greater sensitivity for H_2S and NO_2 with temperature of 250 – 300 °C. The Au:TiO_2/PS films exhibit gradual raise in gas sensitivity, reaching a maximum sensitivity about 42.69% at 300 °C of 64.5 ppm NO_2 gas responsivity.

Similar results are achieved when H_2S is employed as the investigating gas: the optimum sensitivity of the Au:TiO_2/PS film at 1000 mJ gas sensor to 12.6 ppm of H_2S may achieve at 94.12%, and the optimal sensor temperature of the Au:TiO_2/PS sensing is around 250° C. Tables 2 and 3.

There are difference in reaction times and recovery period for various laser ablation energy as a function of working temperature. The time recovery is the time that it takes for the specimen to back to its initial state, in other words the specimen state before pumping the gas, and the response time seems to be the time it takes for the specimen to respond to the gas.

Table 2 R(Ω) values for Au:TiO_2 NPs/PS specimen prior and next NO_2 exposure gas, the sensitivity (percent), response, and recover times(sec) at several laser energies

Samples	T (°C)	$R_{(on)}$ Ω	$R_{(off)}$ Ω	S %	Response time (sec)	Recover time (sec)
Au:TiO_2(600 mJ)/PS	100	3.21	3.64	13.396	34.2	84.6
	200	1.012	1.211	19.664	21.6	68.4
	300	0.965	1.31	35.751	29.7	41.4
Au:TiO_2 (800 mJ)/PS	30	0.418	0.302	27.751	24.3	135
	80	0.221	0.13	41.176	32.4	128.7
	130	67.2	56.9	15.327	22.5	94.5
	200	23.26	21.45	7.782	12.6	48.6
Au:TiO_2(1000 mJ)/PS	200	1.459	1.135	22.207	21.6	47.7
	250	6.21	4.54	26.8921095	10.8	52.2
	300	23.33	13.37	42.69181312	9	62.1

Table 3 R(Ω) values for Au:TiO_2 NPs/PS specimen before and after H_2S gas exposure sensitivity (percent), response, and recover times(sec) at several laser energies

Samples	T (°C)	R(on) Ω	R(off) Ω	S %	Response time (sec)	Recover time (sec)
Au:TiO_2 (600 mJ)/PS	100	4.03	4.43	9.029	38.7	146.7
	200	1.079	1.211	10.900	20.7	61.2
	300	1.245	1.522	18.200	24.3	45
Au:TiO_2 (800 mJ)/PS	30	0.333	0.468	28.846	15.3	226.8
	80	0.125	0.187	33.155	15.3	190.8
	130	65.6	75.5	13.113	7.2	148.5
	200	23.85	24.27	1.731	37.8	76.5
Au:TiO_2 (1000 mJ)/PS	200	11.14	9.98	10.413	26.1	45
	250	36.8	2.161	94.128	7.2	108.9
	300	22.35	1.659	92.577	10.8	100.8

The response and recovery cycles of Au:TiO_2 NPs toward 64.5 ppm NO_2 and 12.6 ppm H_2S, air mixed ratio have been explored. The results are shown in Fig. 6. Response and recovery times of devices were calculated and are indicated in Tables 2 and 3.

Conclusions

In this works, laser ablation of Au:Ti target immersed in (CTAB) solution is a promising and environmentally friendly method for preparing Au:TiO_2NPs. As deduced by their XRD and TEM analysis and AFM properties were employed to characterize the samples. The enhancement in sensitivity of gas sensor increases, with increases the laser energy used to ablate an Au:TiO_2 nanoparticles deposited on PS. The gas sensor should be highly selective when it comes to analytic gas. As a result, we evaluated an Au:TiO_2 NPs/PS thin film gas sensor for various gases at various concentrations, including H_2S and NO_2. The Au:TiO_2 NPs/PS thin film sensor has a better response to H_2S gas, with a response of 94.12% when exposed to 12.6 ppm H_2S.

References

1. N. Abdulkhaleq, U. Nayef, A. Albarazanchi, MgO nanoparticles synthesis via laser ablation stationed on porous silicon for photoconversion application. Optik **212**, 164793 (2020)
2. H. Hussein, U. Nayef, A. Abdul Hussien, Synthesis of graphene on porous silicon for vapor organic sensor by using photoluminescence. Optik **180**, 61–70 (2019)
3. N. Abdulkhaleqa, A. Hasan, U. Nayef, Enhancement of photodetectors devices for silicon nanostructure from study effect of etching time by photoelectrochemical etching Technique. Optik **206**, 164325 (2020)
4. R. Jamal, F. Mutlak, F. Ibrahim, U. Nayef, Synthesis of Ag_2O films by pulsed laser deposited on porous silicon as gas sensor application. Optik **218**, 164971 (2020)
5. D. Jwied, U. Nayef, F. Mutlak, Synthesis of C: Se (core:shell) nanoparticles via laser ablation on porous silicon for photodetector application. Optik **231**, 166493 (2021)
6. U. Nayef, I. Khudhair, Study of porous silicon humidity sensor vapors by photoluminescence quenching for organic solvents. Optik **135**, 169–173 (2017)

7. N. Abdulkhaleqa, A. Hasan, U. Nayef, Enhancement of photodetectors devices for silicon nanostructure from study effect of etching time by photoelectrochemical etching Technique. Optik **206**, 163 (2020)
8. H. Abid, U. Nayef, F. Mutlak, Preparation and characterization Co_3O_4 nanoparticles on porous silicon for humidity sensor by photoluminescence. Optik **178**, 379–383 (2019)
9. Z. Jin, H. Zhou, Z. Jin, R. Savinell, C. Liu, Application of nano-crystalline porous tin oxide thin film for CO sensing. Sens Actuat B-Chem **52**(1–2), 188–194 (1998)
10. X. Tian, X. Cui, T. Lai, J. Ren, Z. Yang, M. Xi, B. Wang, X. Xiao, Y. Wang, (2021). Gas sensors based on TiO_2 nanostructured materials for the detection of hazardous gases: A review. Nano Mater Sci, 5
11. U. Nayef, K. Hubeatir, Z. Abdulkareem, Ultraviolet photodetector based on TiO_2 nanoparticles/porous silicon hetrojunction. Optik **12**(5), 2806–2810 (2016)
12. S. Khudiar, U. Nayef, F. Mutlak, Preparation and characterization of ZnO nanoparticles via laser ablation for sensing NO_2 gas. Optik **246**, 167762 (2021)
13. P. Samarasekara, N. Kumara, N. Yapa, Sputtered copper oxide (CuO) thin films for gas sensor devices. J Phys :Condens Matter **18**(8), 2417 (2006)
14. J. Bai, B. Zhou, Titanium dioxide nanomaterials for sensor applications. Chem Rev **114**(19), 10131–10176 (2014)
15. X. He et al., Metal-organic frameworks derived C/TiO_2 for visible light photocatalysis: simple synthesis and contribution of carbon species. J Hazard Mater **403**, 124048 (2020)
16. T. Li et al., Anatase TiO_2 nanorod arrays as high-performance electron transport layers for perovskite solar cells. J Alloys Compd **849**, 156629 (2020)
17. N. Chinh, C. Kim, D. Kim, UV-light-activated H_2S gas sensing by a TiO_2 nanoparticulate thin film at room temperature. J Alloy Compound **778**, 247–255 (2018)
18. A. Davoodi, M. Babaiee, M. Pakshir, Imitating seasonal temperature fluctuations for the H_2S corrosion of 304L and 316L austenitic stainless steels. Metal Mater Int **19**(4), 731–740 (2013)
19. A. Alonso-Tellez, D. Robert, N. Keller, V. Keller, A parametric study of the UV-A photocatalytic oxidation of H2S over TiO_2. Appl Catal B Environ **115**, 209–218 (2012)
20. S.K. Pandey, K.-H. Kim, K.-T. Tang, A review of sensor-based methods for monitoring hydrogen sulfide. TrAC Trends Anal Chemi **32**, 87–99 (2012)
21. G.N. Chaudhari, D.R. Bambole, A.B. Bodade, P.R. Padole, Characterization of nanosized TiO_2 basedH2S gas sensor. J Mater Sci **41**(15), 4860–4864 (2006)
22. Z. Zhu, S.-J. Lin, C.-H. Wu, R.-J. Wu, Synthesis of TiO_2 nanowires for rapid NO_2 detection. Sens Actuat: A Phys **272**, 288–294 (2010)
23. U.M. Nayef, R.I. Kamel, Bi_2O_3 nanoparticles ablated on porous silicon for sensing NO_2 gas. Optik **208**, 164146 (2020)
24. D. Jwied, U. Nayef, F. Mutlak, Synthesis of C: Se nanoparticles ablated on porous silicon for sensing NO2 and NH3 gases. Optik **241**, 167013 (2021)
25. F.M. Liu, Y.H. Guan, H.B. Sun, X.M. Xu, R.Z. Sun, X.S. Liang, P. Sun, Y. Gao, G.Y. Lu, YSZ-based NO_2 sensor utilizing hierarchical In_2O_3 electrode. Sens Actuator B: Chem **222**, 698–706 (2016)
26. S.S. Shendage, V.L. Patil, S.A. Vanalakar, S.P. Patil, N.S. Harale, J.L. Bhosale, J.H. Kim, P.S. Patil, Sensitive and selective NO_2 gas sensor based on WO_3 nanoplates. Sens Actuator B: Chem **240**, 426–433 (2017)
27. B. Feizi Mohazzab, B. Jaleh, O. Kakuee, A. Fattah-alhosseini, Formation of titanium carbide on the titanium surface using laser ablation in n-heptane and investigating its corrosion resistance. Appl Surf Sci **478**, 623–635 (2019)
28. M. Jabir, U. Nayef, W. Abdulkadhim, Z. Taqi, G. Sulaiman, U. Sahib, A. Al-Shammari, Y. Wu, M. El-Shazly, C. Su, Fe_3O_4 nanoparticles capped with PEG induce apoptosis in breast cancer AMJ13 cells via mitochondrial damage and reduction of NF-κB translocation. J Inorg Organomet Polym Mater **313**, 1241–1259 (2021)
29. A. De Giacomo, M. Dell'Aglio, A. Santagata, R. Gaudiuso, O. De Pascale, P. Wagener, G.C. Messina, G. Compagnini, S. Barcikowski, Cavitation dynamics of laser ablation of bulk and wire shaped metals in water during nanoparticles production. Phys Chem Chem Phys **15**(9), 3083–3092 (2013)
30. R. Kamel, D. Ahmed, U. Nayef, Synthesis of Bi_2O_3 nanoparticles by laser ablation on porous silicon for photoconversion application. Optik **193**, 163013 (2019)

Publisher's Note Springer Nature remains neutral with regard to jurisdictional claims in published maps and institutional affiliations.